Vision Research 211 (2023) 108208

Contents lists available at ScienceDirect

Vision Research

journal homepage: www.elsevier.com/locate/visres

Fine-scale measurement of the blind spot borders

Annegret Meermeier [a,b], Markus Lappe [a,b], Yuanhao H. Li [c,d], Katharina Rifai [e], Siegfried Wahl [e,f], Michele Rucci [c,d]

[a] Institute for Psychology, University of Muenster, Muenster, Germany
[b] Otto Creutzfeldt Center for Cognitive and Behavioral Neuroscience, University of Muenster, Muenster, Germany
[c] Department of Brain & Cognitive Sciences, University of Rochester, New York, USA
[d] Center for Visual Science, University of Rochester, New York, USA
[e] Carl Zeiss Vision International GmbH, Aalen, Germany
[f] Institute for Ophthalmic Research, University Tübingen, Tübingen, Germany

A B S T R A C T

The blind spot is both a necessity and a nuisance for seeing. It is the portion of the visual field projecting to where the optic nerve crosses the retina, a region devoid of photoreceptors and hence visual input. The precise way in which vision transitions into blindness at the blind spot border is to date unknown. A chief challenge to map this transition is the incessant movement of the eye, which unavoidably smears measurements across space. In this study, we used high-resolution eye-tracking and state-of-the-art retinal stabilization to finely map the blind spot borders. Participants reported the onset of tiny high-contrast probes that were briefly flashed at precise positions around the blind spot. This method has sufficient resolution to enable mapping of blood vessels from psychophysical measurements. Our data show that, even after accounting for eye movements, the transition zones at the edges of the blind spot are considerable. On the horizontal meridian, the regions with detection rates between 80% and 20% span approximately 25% of the overall width of the blind spot. These borders also vary considerably in size across different axes. These data show that the transition from full visibility to blindness at the blind spot border is not abrupt but occurs over a broad area.

1. Introduction

The punctum caecum or blind spot is a disruption of visual input. Located approximately 15 to 20 degrees in the temporal periphery, it corresponds to the region on the retina at which the optic nerve leaves the eye and no photoreceptors exist. It has a roughly oval shape given by the optic disc, the optic nerve head, and ranges in length from 5° to 7° on the horizontal meridian and from 7.5° to 10° on the vertical meridian (Armaly, 1969; Chamlin, 1960; Dolderer, Vontheim, Johnson, Schiefer, & Hart, 2006; Rhodes, 2013; Safran, Mermoud, Weisse, & Desangles, 1993). Thus, the blind spot spans a considerable fraction of the visual field, more than 50 times the area covered by the foveola—the high-acuity portion of the retina.

Given the size and position of the blind spot, it is remarkable that humans are normally unaware of this vast region lacking visual information only a few degrees away from their center of gaze. As it happens with pathological (Zur & Ullman, 2003; Murakami, Komatsu, & Kinoshita, 1997; Wittich, Overbury, Kapusta, Watanabe, & Faubert, 2006; Stefani et al., 2011) and artificially-induced scotomas (Ramachandran & Gregory, 1991; Weil, Kilner, Haynes, & Rees, 2007; Chen et al., 2019), this effect appears to be mediated by filling-in mechanisms, by which the visual system infers spatial continuity based on information acquired in the surrounding regions. It is, therefore, not surprising that the blind spot has been studied extensively to examine the mechanisms of perceptual filling-in and the assumptions that the visual system uses in this process (Ramachandran, 1992; Komatsu, Kinoshita, & Murakami, 2000; Spillman et al., 2006; Komatsu, 2006; Raman & Sarkar, 2016)

While it is clear that the visual system is extremely efficient in applying Gestalt principles in this region, it remains unknown how exactly visibility degrades into blindness at the blind spot borders. Measuring this transition is complicated by several factors. A major challenge is provided by eye movements, as humans are incapable of maintaining steady gaze (Rolfs, 2009; Kowler, 2011; Rucci & Poletti, 2015). Two types of eye movements are present during fixation: small saccades, known as microsaccades, occur every few hundreds of milliseconds, normally moving both eyes (Krauskopf, Cornsweet, & Riggs, 1960; Fang et al., 2018) toward nearby objects of interest (Ko, Poletti, & Rucci, 2010; Poletti, Intoy, & Rucci, 2020). In the intervals between saccades and microsaccades, the eyes wander erratically with instantaneous speed typically under 2°/s when the head is immobilized and faster when the head is free to move normally (e.g., Poletti, Aytekin, & Rucci, 2015). These movements complicate mapping of visibility, since a probe at a fixed position in space will at times fall onto the functioning retina and sometimes on the optic disc. Thus, leaving fixational eye movements unaccounted for will result in spatial smearing of the transition zones.

Another major challenge to precisely estimate visibility at the blind spot edges is provided by the very mechanisms of filling-in, which affect performance in ways that depend on the characteristics of visual

https://doi.org/10.1016/j.visres.2023.108208
Received 13 July 2022; Received in revised form 4 December 2022; Accepted 20 February 2023
Available online 14 July 2023

stimulation. The spatial structure of the probe used to test visibility plays a critical role. Given that acuity is low at the eccentricity of the blind spot, it is tempting to use relatively large probes. But using large stimuli is clearly a problem, as the area of the blind spot, including its border, is represented in the visual cortex by relatively large receptive fields (Awater, Kerlin, Evans, & Tong, 2005; Fiorani, Rosa, Gattass, & Rocha-Miranda, 1992), some of which span the entire region (Azzi, Gattass, Lima, Soares, & Fiorani, 2015; Fiorani et al., 1992). Large stimuli may reach the border of the blind spot even if their center is well inside the blind area, leading to overestimation of the transition regions. In fact, it is already established that large, high-contrast stimuli lead to a smaller estimate of the blind spot area than small, low-contrast ones (Dolderer et al., 2006). This problem is further complicated by the observation that perceptual filling-in is also elicited by narrow stimuli if they extend in space, for example a sufficiently long line thinner than 4′ (Spillmann, 2006).

The temporal characteristics of the probe are also important. Two main methods have been applied, static and dynamic, depending on whether subjects judge the visibility of stationary probes or report the appearance/disappearance of probes moving at constant speeds. In this latter procedure, since the measurement relies on the ability of the participant to report a temporal event (e.g., the probe becomes visible traveling out of the blind spot), its resolution depends on the reaction time, which is known to differ widely both across participants and, for a given individual, across trials. Modern optometric devices attempt to correct for reaction time, hereby increasing the precision of the data (Dolderer et al., 2006), but this correction cannot eliminate individual inter-trial variability. Furthermore, kinetic protocols are complicated by the different perceptual mechanisms involved in detecting the disappearance and the reappearance of the probe. For example, predictive mechanisms may prolong visibility of the probe even when it is already within the blind spot, artificially shrinking the region of blindness (Maus & Nijhawan, 2008; Maus & Whitney, 2016).

As these observations emphasize, careful examination of the unfolding of the transition between visibility and blindness at the blind spot boundaries requires consideration of eye movements as well as the perceptual mechanisms of filling-in and predictions. In this study, we describe an approach that relies on high-resolution eye-tracking, fine localization of the line of sight, and real-time gaze-contingent control of retinal stimulation. This method eliminates most of the confounds described above, enabling mapping of visibility around the blind spot with higher precision.

2. Methods

2.1. Participants

Twelve subjects (20–28 years old, 3 males) participated in the experiments. All participants took part in measurements of the blind spot borders on the horizontal meridian. Two of them also participated in measurement along the vertical meridian. All participants were emmetropic, with at least 20/25 acuity in a Snellen test. Subjects gave informed written consent and were compensated for their participation. The study was approved by the institutional review board at the University of Rochester and adhered to the tenets of the declaration of Helsinki.

2.2. Apparatus

Retinal stabilization was provided by EyeRIS (Rucci, Iovin, Poletti, & Santini, 2007; Santini, Redner, Iovin, & Rucci, 2007), a custom system for gaze-contingent display that operated in conjunction with a high-resolution eye-tracker. This hardware/software system guarantees precise synchronization between eye movement data and the refresh of the image on the monitor. Eye movements were measured by means of two Dual Purkinje Image (DPI) eye-trackers. These systems compare the motion of the first and fourth Purkinje Images of an infrared beam, yielding a resolution of approximately 1′ (Ko, Snodderly, & Poletti, 2016). Data from 7 observers were acquired by means of a Generation 6 DPI (Fourward Technologies). They were low-pass-filtered at 500 Hz, and sampled at 1 kHz. This device has an internal time delay of 0.25 ms and root mean square noise level measured by means of an artificial eye of less than 20″ (Crane & Steele, 1985). The eye movements of the other 5 participants were measured at 340 Hz by means of a recently developed digital version of this machine, a digital Dual Purkinje Image eye-tracker (dDPI; Wu et al., 2023). In both setups, participants were seated on a chair in a dimly illuminated room, while movement of the head was minimized by using a custom-fitted, dental-imprint bite bar and a head rest. Vertical and horizontal eye position data were recorded for subsequent analysis.

2.3. Gaze localization

Accurate localization of the line of sight was achieved by means of a gaze-contingent calibration procedure described in detail in previous publications (Poletti & Rucci, 2016). In this procedure, participants used a joypad to fine-tune the parameters of a pre-estimated calibration. They sequentially fixated on a series of fixation markers and adjusted the estimated position of the line of sight, which was displayed in real-time on the monitor. The offsets inserted by the participants were iteratively incorporated in the bilinear transformation that mapped the eye-tracker output into pixel coordinates on the display. This procedure has been shown to improve the accuracy of gaze localization by one order of magnitude, therefore enabling accurate mapping of the position of the blind spot region within the visual field. Gaze-contingent calibration was also repeated at the center of the screen after every block of 10 trials, to counteract possible misalignments due to small residual head movements and other possible causes.

2.4. Stimuli

Visibility was probed using maximum-contrast squared dots with a side length of 2′, which were presented at the desired eccentricity relative to the center of gaze. Probes were briefly flashed (14 ms) on a ROG Swift PG278Q Gaming Monitor (27″) at a resolution of 2560 × 1440 and refresh rate of 144 Hz. The monitor was positioned at distance of 75 cm from the eye in the dDPI experiments, and at 115 cm in the DPI recordings, resulting in pixel resolution of 0.9′ and 0.6′, respectively. The longer distance in the experiments with the digital dDPI was necessary to optimize eye-tracking and avoid that background light emitted from the monitor would interfer with the tracking quality. Participants viewed the stimuli monocularly with the right eye while the left eye was patched.

2.5. Blind spot mapping

Subjects were asked to report the appearance of probes displayed at various locations around and within the blind spot. We first made sure that participants could reliably detect the probe even at the greatest eccentricities. Full visibility of the probe at all eccentricities was necessary to exclude any possible bias due to a decline in performance with increasing eccentricity. Participants were instructed to maintain stable fixation on a marker (dotted circle) displayed at a fixed location of the display (see Fig. 1a).

A trial started with the appearance of the fixation marker. After a variable interval of 500–1100 ms, a test probe was briefly flashed (14 ms) at the desired location. The probe was always presented under retinal stabilization, ensuring precise control of the stimulus position on the retina. The fixation marker stayed on for another 300 ms after presentation of the probe and was then replaced by a red dot. The appearance of the red dot acted as a prompt for participants to enter their response on whether they saw the stimulus. Perceptual responses

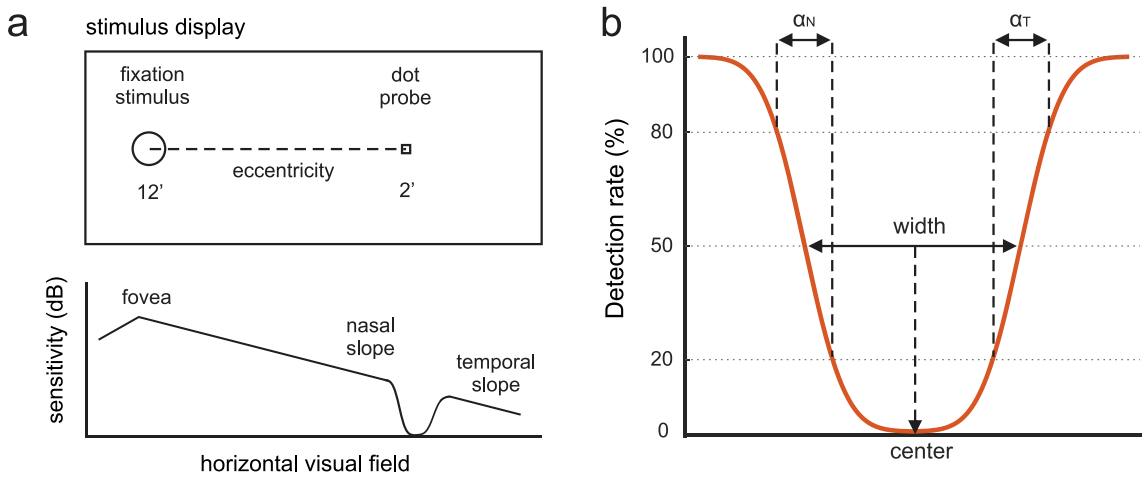

Fig. 1. Approach and terminology used in this study. **(a)** Procedure for testing visibility around the blind spot. The upper graph represents sensitivity across the visual field. The bottom panel is a sketch of the stimulus display. Subjects maintained fixation on a 12′-diameter circle, while small high-contrast probes (2′ squares) were displayed at desired locations on the retina. **(b)** Definition of the blind spot's width, center, and border extents: α_N and α_T represent the widths of the nasal and temporal edges, respectively. Detection rates of 20%, 50% and 80% were determined from fitted psychometric functions.

were registered via button presses on a joypad.

A coarse-to-fine procedure was used for locating the blind spot and mapping its borders. This procedure consisted of four stages, each based on the method of constant stimuli applied at a different scale. In the first stage, 12 positions equispaced by 1 deg were tested 3 times. In the second stage, 11 positions at 0.2 deg steps were repeated twice. In the third stage, 25 positions separated by just 2 pixel (1.2′ or 1.8′ depending on the setup) were presented twice. These three steps were used to provide a first approximate estimation of the location of the blind sport borders, so to narrow the area that was then examined at high resolution. This occurred in fourth stage of the procedure, when probes specifically targeted the transition zones of visibility at the margins of the

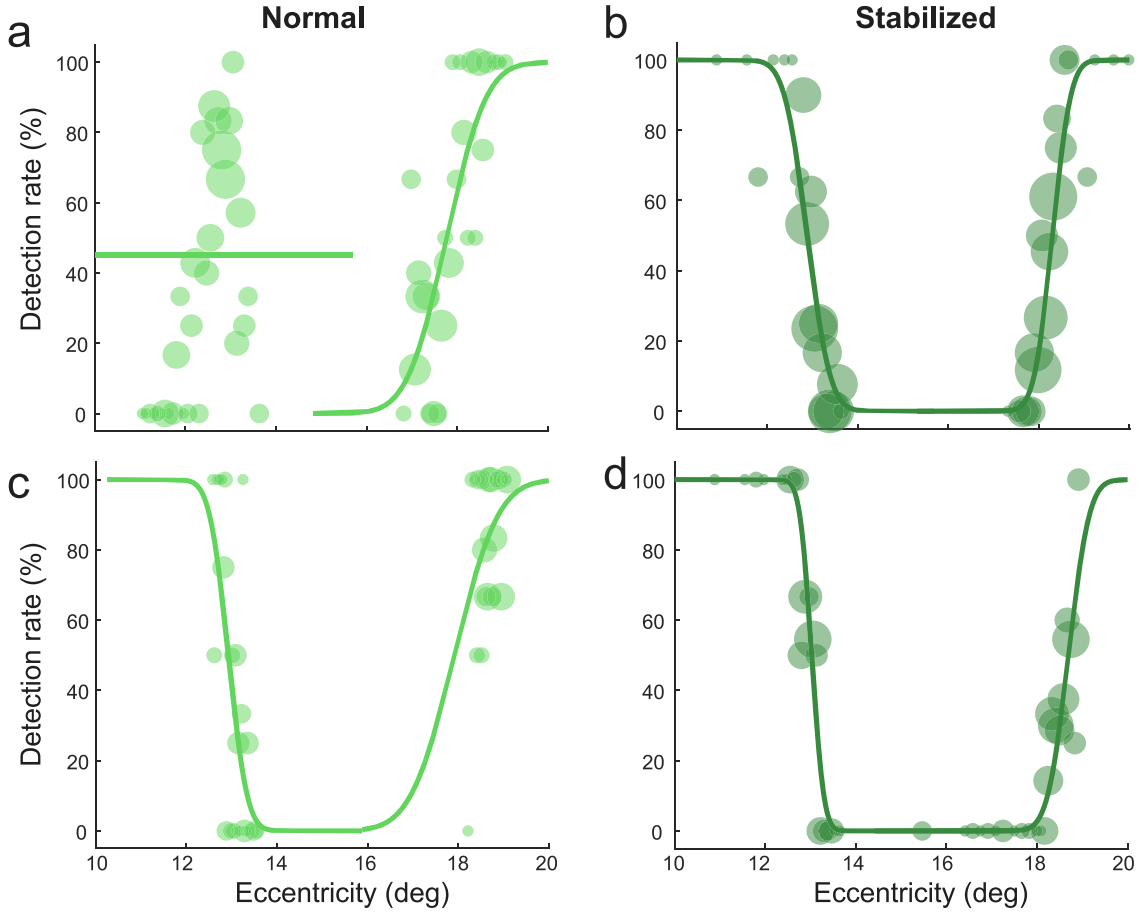

Fig. 2. Horizontal blind spot borders measured for two participants with and without compensation for fixational eye movements. Open circles represent estimated sensitivity at various retinal locations. The solid line is the resulting psychometric fit. The two rows show data from different subjects. Measurements obtained with and without retinal stabilization are shown in the panels on the right and left columns, respectively.

blind spot. In all stages, probes were presented in random order across the possible locations. The same procedure was applied for measurements along all axes. To ensure that participants remained vigilant and complied with the task, catch trials were interspersed with normal trials. In the catch trials, the probe was flashed far outside the blind spot, at 7.5 deg eccentricity from the fovea. In the data reported in this study, participants always reported full visibility of these probes.

To provide quantitative examples of the consequences of not considering fixational eye movements, for two observers we also mapped visibility without compensating for the smearing of spatial measurements caused by fixational eye movements. These data are compared in Fig. 2 to those obtained with oculomotor compensation, when confounds from eye movements were eliminated by presenting stimuli at fixed positions relative to the line of sight. Considerable numbers of trials were collected to ensure rigorous comparisons, approximately 260 trials in each condition for one subject and 150 trials for the other participant.

For one observer, we systematically probed visual sensitivity in the entire space surrounding the blind spot. To this end, we used the approach described above along 60 evenly-spaced angular axes intersecting the blind spot center. Probe positions were more densely placed near the borders of the blind spot and more coarsely in the surrounding functional areas of the retina. Psychometric functions were individually estimated on each axis as to quantify the widths of the border regions along various orientations. To obtain a full two-dimensional map of visibility, performance in between the tested locations was then spatially interpolated using cubic spline functions, first along each axis and then across circular trajectories. This latter step was performed on circles with increasing radii from the blind spot center and alternating directions of interpolation (clock-wise vs. counterclock-wise) to limit artifacts in the fitting. The resulting image was then smoothed using a 6′ by 6′ median filter. Interpolation based on the original visibility data points rather than the psychometric functions obtained on each individual axis enabled better fitting of experimental data in 2D space. Overall, the map shown in Fig. 6 was obtained using over 17,653 trials collected over multiple days.

For this subject, we confirmed that the map of visibility closely matches the anatomical substrate by comparing the results of our procedure with the anatomical data obtained by two other measurements of the blind spot: an image of the fundus of the eye and a 9 mm high-definition scan of the retina obtained via optical coherence tomography. The latter was recorded by means of a CIRRUS 5000 without additional lenses and with default settings for the fixation cross. The correspondence between perceptual and anatomical measurements is emphasized in Fig. 6b by overlaying the estimated perceptual map on the fundus image. The reference frames of the two images were brought in register by manual rotation and scaling.

2.6. Data analysis

Only periods with uninterrupted tracking and without blinks were selected for data analysis. Eye movements with speed higher than 3°/s and amplitude larger than 3′ were classified as possible saccadic events. If the eye velocity exceeded 2°/s during the 100-ms interval before and after the presentation of the probe, the trial was discarded to avoid possible errors in positioning the probe. Periods of blinks were automatically removed from data analysis. If a recalibration trial indicated a shift in accuracy in gaze localization of more than 10′, calibration was judged as having decayed substantially, and all trials acquired since the previous recalibration were discarded.

Data were analyzed using MATLAB (the Mathworks, Nattick, MA) to estimate the widths and slopes of the transition zones as well as the overall width and center eccentricity of the blind spot (see Fig. 1b). Specifically, each transition zone was estimated by fitting via a maximum-likelihood procedure (Wichmann & Hill, 2001a) the data collected at the corresponding eccentricities surrounding the border. The width of this region was defined as the difference between the 20% and 80% performance thresholds given by the psychometric curves. This parameter is indicated by α in the following of this article. Variability of the psychometric functions was assessed by means of parametric bootstrap (N = 500) to obtain the standard deviation of the parameters. The goodness of fit was evaluated by means of the log-likelihood ratio (Wichmann & Hill, 2001b).

The center of the horizontal blind spot was estimated as the mean between the temporal and nasal locations yielding 50% performance. The width of the blind spot was correspondingly calculated as the distance between these two points. All measurements are given in angular coordinates of the visual field relative to the line of sight, so that the nasal blind spot border identifies the border closest to central fixation in the visual field. An analogous procedure was followed for processing vertical measurement data, with the axis directions oriented upward, from the lower border of the blind spot toward the upper one.

3. Results

The human eyes move incessantly. We are normally not aware that eye movements continually shift the projection of stimuli on the retina even during careful fixation. These movements vary widely across individuals and can cover an area as large as the entire foveola (Cherici, Kuang, Poletti, & Rucci, 2012). The consequences of fixational eye movements are typically not considered when examining how vision declines at the blind spot edges (Haefliger & Flammer 1991; Meyer, Guhlmann, & Funk, 1997; Wyatt, Dul, & Swanson, 2007). Yet, since the spatial location of the blind spot moves together with the eye, precise mapping of the transition zones of visibility is likely affected.

In this study, we eliminated oculomotor confounds by tracking eye movements at high resolution and compensating in real-time for the shifts that they would cause on the stimulated position on the retina. Subjects were asked to detect tiny probes (2′ dots at maximum contrast) presented at various eccentricities around the edges of the blind spot. However, rather than defining the eccentricity of a probe in monitor coordinates, as commonly done in vision research experiments, eccentricity was here quantified by the angular distance from the center of gaze, a reference frame fixed to the retina. We summarize the width of a transition region by the distance between the estimated 20% and 80% levels of visibility. This distance is indicated as the parameter α in the rest of this article.

To provide examples of the benefit of accounting for oculomotor influences, Fig. 2 shows the transition zones on the horizontal meridian measured for two observers in the presence and absence of compensation for eye movements. Measurements differed considerably in the two conditions, with a smoother progression of data points under retinal stabilization, as evident by visual inspection of the graphs in Fig. 2. In both observers, at least one of the transitions yielded data that could be fitted much more tightly by a monotonic psychometric function when confounds from eye movements were eliminated ($p < 0.03$; bootstrap test for goodness of fit). The resulting uncertainty in the estimation of the slopes of the transition zones was approximately 60% smaller under retinal stabilization (average reduction in standard deviation of the estimated slope from 11.53 to 4.4 arcmin^{-1}).

For one participant, direct mapping yielded such poor data that the transition zone at the nasal edge could not be plausibly fitted by the psychometric function. This happened because, without controlling for eye movements, visibility first abruptly decreased with increasing eccentricity, then increased again before finally dropping to zero (Fig. 2a). In contrast, the width of the transition zone, α_N could be reliably estimated under retinal stabilization, yielding a value of 40′. In this subject, the extent of the temporal edge, α_T, shrunk from 69′ to 32′ by controlling for eye movements. Similarly, in the second subject, α_N and α_T decreased from 33′ and 76′ with direct mapping to 21′ and 36′ under retinal

stabilization. Thus, on average, a 47.5% reduction in the widths of the blind spot borders was observed by properly compensating for eye movements.

These differences in measuring the transition zones also translated into broader discrepancies in the measured position and size of the blind spot. In the first subject, assuming the nasal edge to lie at the mean position of tested locations, the center and width of the region were 15.2° and 5.1°, respectively. These values changed to 15.6° and 5.4° under retinal stabilization. A similar discrepancy occurred for the other subject, with the measurements obtained under retinal stabilization indicating a wider (5.67° vs. 4.98°) and more eccentric blind spot (15.9° vs. 15.4°). Thus, retinal stabilization appears to be an effective method for obtaining more precise measurements and reducing uncertainty in estimating the blind spot borders.

3.1. Horizontal borders of the human blind spot

Following the stabilized procedure described in Fig. 2, we mapped visibility around the blind spot along the horizontal meridian in the right eye of $N = 12$ participants (Fig. 3). On average, the blind spot was centered at an eccentricity of 15.53° ± 0.95° (mean ± standard deviation) and covered a visual angle of 5.30° ± 1.09°. Notably, the measured transitions zones extended considerably even after eliminating confounds from eye movements, yielding an average width of 0.72° ± 0.41°. These are relatively large values if one considers that the overall region of blindness (the region with visibility rates below 20%) was 4.5°. That is, the transition zones in the blind spot extended for an amount equal to approximately one third of the width of the region of blindness. Such gradual edges with declining visibility also imply a much broader region in which vision is perturbed around the blind spot. On average, across observers, the region in which detection rates fell below 80% extended for approximately 6° ± 1.24°.

Comparison of measurements at the two edges indicated that the transition regions on the two sides of the blind spot are similar in size, with $\alpha_N = 0.69° \pm 0.47°$ on the nasal side and $\alpha_T = 0.76° \pm 0.35°$ on the temporal side ($p = 0.56$; t-test for dependent samples). In fact, the measurements at the two edges were correlated with each other ($r = 0.607$, $p = 0.036$, Fig. 4,b c), suggesting that the steepness of the blind spot borders is a feature consistent within an individual. The widths of the transition zones also exhibited a positive correlation with the eccentricity of the blind spot's center (nasal: $r = 0.672$, $p = 0.017$; temporal: $r = 0.626$, $p = 0.029$; Fig. 4d). That is, the steepness of the borders decreased with increasing eccentricity of the blind spot, possibly a consequence of the declining density and increasing size of photoreceptors.

3.2. Vertical border of the human blind spot

In two participants, we applied our method to also measure the vertical dimensions of the blind spot (Fig. 5). To this end, we first mapped visibility across the horizontal meridian and estimated the center of the blind spot on this axis. We then applied the same procedure along the vertical axis intersecting the previously estimated horizontal center. In the first subject, this analysis revealed that the entire blind spot was positioned quite low in the visual field and extended far below the horizontal meridian. It covered more than 11° in visual angle, ranging from 1.53° above the horizontal midline to 9.64° in the lower hemifield. In the other participant, the blind spot was located higher and covered a smaller extent, slightly more than 9°, from 2.73° to −6.34°.

In contrast to the similarity observed between nasal and temporal measurements on the horizontal meridian, the transition zones on the vertical meridian differed greatly at the upper and lower borders. Visibility decayed more gradually in the upper border resulting in larger widths of the transition zones. In the first subject, the transition zone only covered 38′ at the bottom but extended to almost 3° at the top (179′). In the other subject, the measured widths of the transition zones were 19′ at the lower border and 87′ at the upper one. It is likely that these differences were caused from angioscotomas overlapping with the

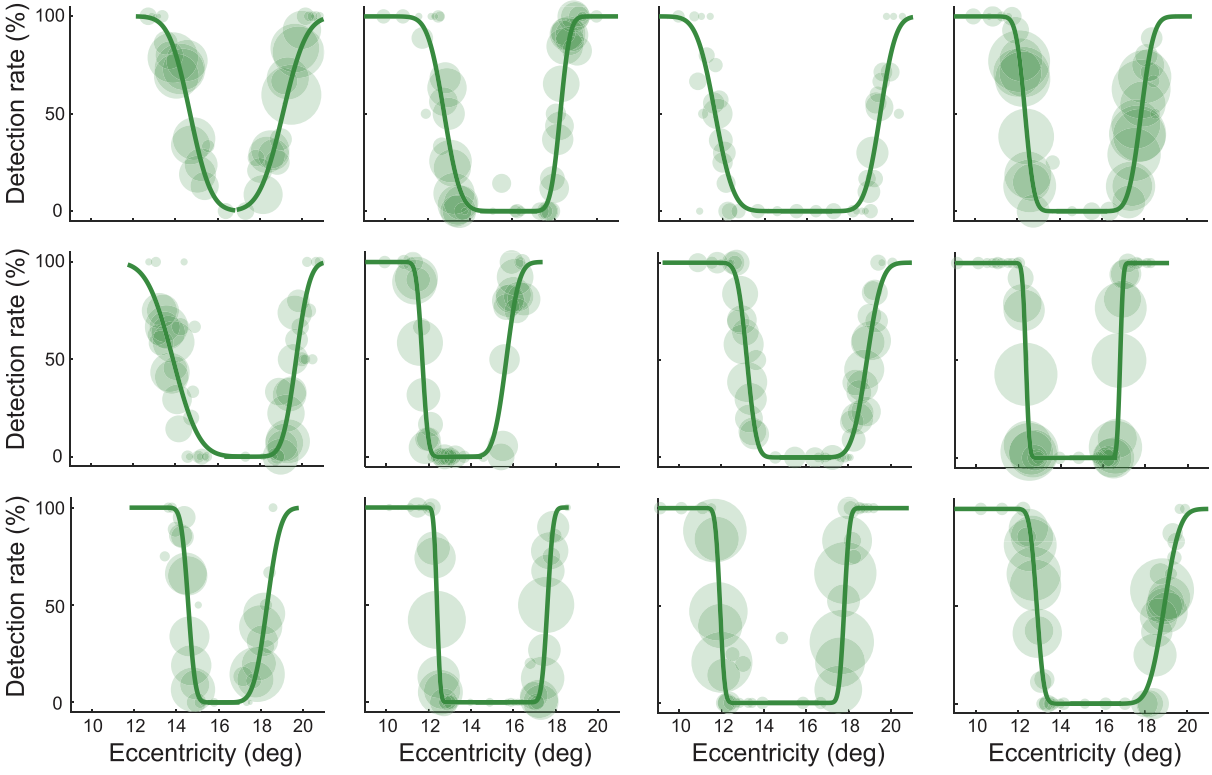

Fig. 3. Individual measurements of the blind spot borders across the horizontal meridian. Each panel shows data from one subject. Graphic conventions are the same as in Fig. 2. All data were collected while compensating for fixational eye movements via high-resolution eye-tracking and gaze-contingent display control.

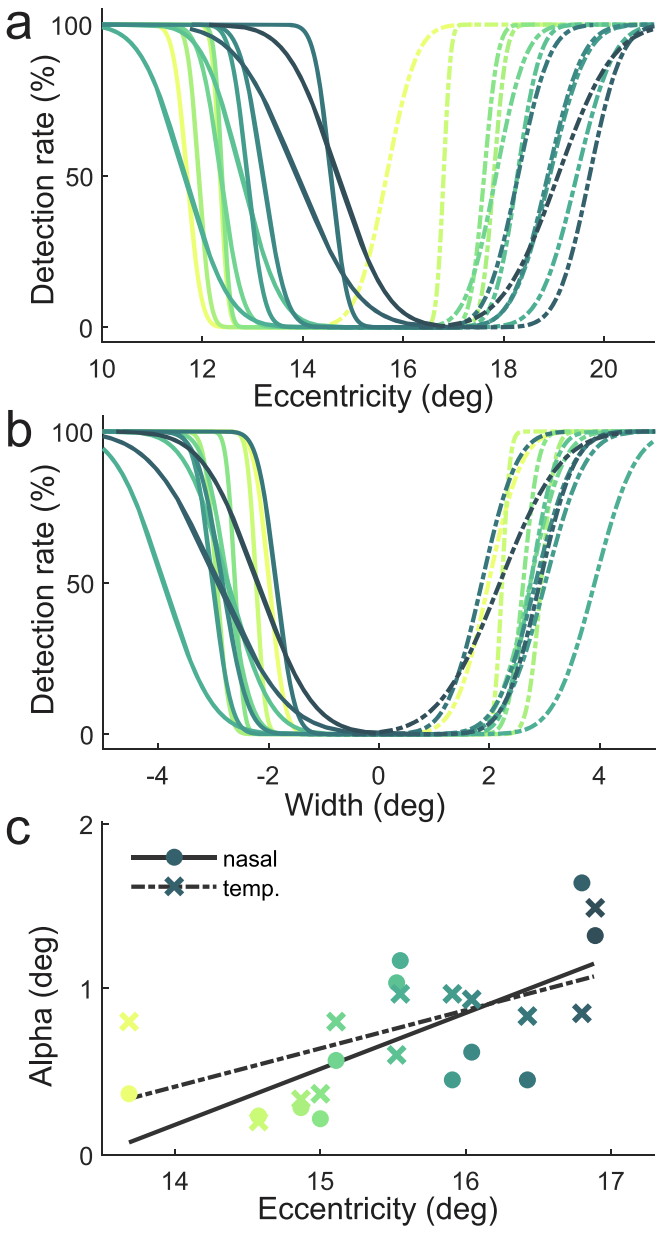

Fig. 4. Summary of all blind spot measurements across the horizontal meridian. **(a)** Overlay of the psychometric functions of all subjects to illustrate the large individual variability in both width and position. **(b)** Same data as in panel **a**, after realigning data relative to the center position of the blind spot. Notes the similar steepness of nasal and temporal borders and the relation between the size of the blind spot and the steepness of its borders. **(c)** Correlation between widths of the nasal and temporal borders and center eccentricity.

vertical border of the blind spot, as major vessels typically exit the human blind spot passing from this point. This idea is supported by the 2D map of the blind spot acquired, using our method, for the subject of Fig. 5b (see Fig. 6), and supports the precision of our approach.

3.3. 2D map of the human blind spot

To further examine visibility around the blind spot, for one participant, we used our approach to test sensitivity across multiple axes at various orientations. This enabled derivation of a two-dimensional map of visibility with estimation of transition zones surrounding the entire blind spot. To this end, we systematically probed visibility along 60 evenly spaced angular axes. Data were then interpolated in 2D space to estimate visibility in between the tested locations.

The result in Fig. 6 shows that the width of the transition zones varied substantially around the blind spot. The median width was 20′, with 25th and 75th percentiles of 14′ and 38′, respectively. This represents an average variation around the median of 61%. The width of the median nasal rim was 16′ (quartiles: 13.4′, 29.9′), whereas the width of the median temporal rim was 27′ (quartiles: 14.8′ and 45.4′) a difference that was not statistically significant (z=-0.966, p =0.33; Wilcoxon sign rank test). On average, the superior edge of the blind spot extended for 89′, whereas the inferior edge was 34′ wide. On the diagonal axes, the measured widths were 30′ in the 45 deg direction, 17′ in the 135 deg direction, 15′ at 225 deg and 31′ at 315 deg.

To confirm that these large fluctuations in the widths of the transition zones were partly caused by angioscotomas, for this participant we collected images of the eye fundus and compared them to our psychophysical measurements (Fig. 6b). Although the two measurements differ in their reference frames (visual angles for the psychophysical measurements, retinal coordinates for the fundus image) and small rotational misalignments may be present, a strong similarity between the participant's functional measurements and the underlying anatomical structure is clearly visible. Note that the directions which yielded broader transition zones as measured psychophysically correspond with those in which vessels are present in the fundus image. For example, the vertical borders of the blind spot closely match the positions of major vessels leaving the optic nerve head, which are likely to be responsible for large angioscotomas.

To gain further information on the correspondence between psychophysical measurements and retinal anatomy, for this subject we also acquired a high-resolution tomographic scan of the retina using a Cirrus HD-OCT. The 9 mm horizontal image in Fig. 7a shows not only the fovea but also the nasal border of the blind spot. For these images a conversion of pixels to optical angles allows registration of the functional data with the underlying substrate. The entire 9 mm image spanned a visual angle that ranged from -15.705° to +15.705°. This resulted in a factor of 0.21′/pix, which we then used to overlay psychophysical measurements on the image.

The image shown in Fig. 7a is the retinal tomographic section corresponding to the meridian axis that was probed psychophysically. Fig. 7b shows an enlargement of the specific region in which visibility was tested (gray rectangle in Fig. 7a). Overlaid in green is the participant's detection performance for stimuli around the blind spot border. As shown by these data, the location at which visibility drops coincides with the anatomical locus at which the different layers of the retina, and especially the photoreceptor layers (see Fig. 7 red arrow), become discontinued. These results further confirm that our approach is highly precise in estimating the location of the blind spot. Although the resolution of these data does not allow assessment of whether photoreceptors progressively decline in the transition zone, a decline in visibility appears to initiate at a location in which the photoreceptors outer segments are already disrupted. Thus, the alignment obtained in this analysis is compatible with the idea that a decline in performance is mediated by increasing axonal convergence and/or lateral connections with increasing eccentricity.

4. Discussion

We measured visibility around the blind spot with high-resolution perimetry under retinal stabilization. This approach compensates for the influences of the incessant eye movements that humans perform while attempting to maintain steady fixation. Since these movements shift gaze by amounts larger than the widths of the transition zones at the blind spot borders, retinal stabilization removes a critical source of measurement noise. We show that even after eliminating this oculomotor confound, the transition from visibility to blindness takes place over a considerable spatial extent. With the temporal and nasal borders

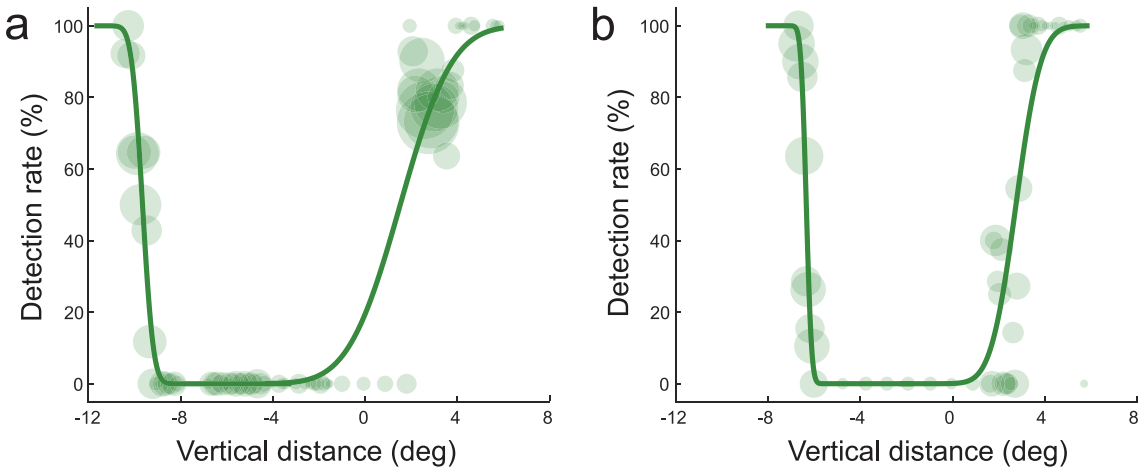

Fig. 5. Vertical borders of the blind spot in two participants. Measurements were obtained on the vertical axis intersecting the blind spot center on the horizontal meridian, which was previously estimated. Data are plotted as a function of distance from this point.

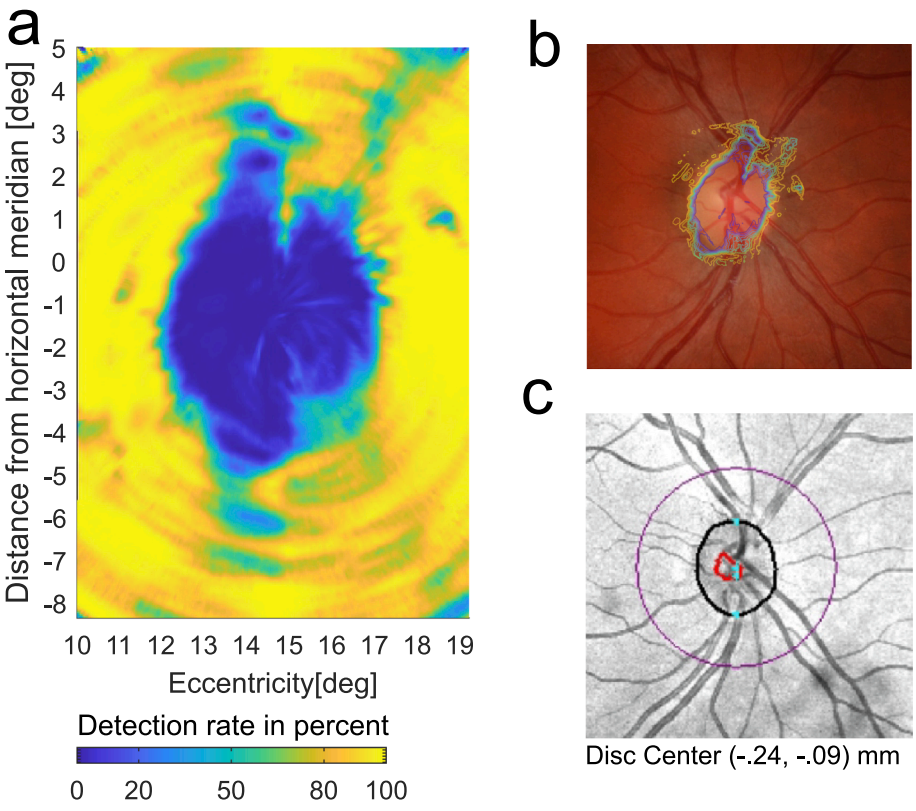

Fig. 6. Comparison between psychophysical measurements and imaging of the blind spot. **(a)** Two-dimensional map of visibility around the blind spot for one participant. The map covers the entire blind spot region in the right eye as well as the adjacent surrounding portion of visual space. **(b)** Fundus image from the same eye showing the optic disc (light colored oval) and major vessels. Note the correspondence between the areas of impaired visibility and the locations of visible vessels, suggesting that these are indeed angioscotomas. The visibility map (blue/yellow edges), manually rotated and scaled, is here superimposed on the fundus to facilitate comparison. **(c)** Image of the blind spot as produced by the Cirrus 5000 HD-OCT. Dimensions are in millimeters.

of the blind spot each occupying about 0.7° of visual angle, their combined width is about 25% of the total horizontal dimension of the blind spot (about 5°).

The approach described in this study allows for mapping of visual sensitivity with unprecedented accuracy. This was the result of combining several precautions. First, our method relied on probes that were highly localized in both space and time and yet reliably detected—at ceiling performance—outside the blind spot region. Probes extended for only 2′ and 14 ms and were presented at random locations to avoid possible influences of prediction mechanisms. Second, we compensated for the effects of eye movements with high precision. The resolution of the DPI eye-tracker is approximately 1′ (Ko et al., 2016) and the online stabilization protocol was here executed at 144 Hz. Since we discarded all trials with microsaccades and all trials with eye speed above a low threshold (120′/s), the remaining spatial uncertainty due to eye movement was less than 1′ (about 0.84′; median error 0.35′). Third, absolute measurements of eccentricity was also very accurate, as our gaze-contingent calibration improves localization of the origin of the coordinate system (the center of gaze) by approximately one order of magnitude over standard methods (Poletti & Rucci, 2016).

As often done in tests of visual field perimetry, we mapped visibility via a simple detection task, a straightforward procedure in which observers directly reported whether a probe was visible. A possible concern is whether this procedure contributed to variability across subjects because of individual biases in response criteria. Changes in response biases would indeed affect the overall estimated width of the blind spot. However, as long as these biases remain constant across the tested locations on the retina, they would not affect the estimated width of the

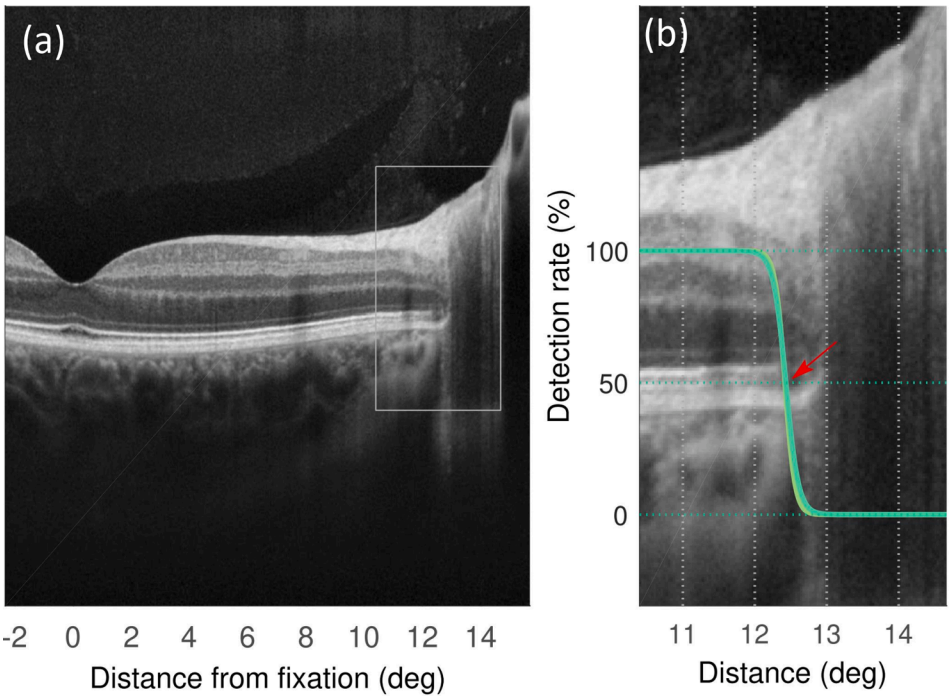

Fig. 7. Comparison between psychophysical measurements and tomographic imaging of the retina. **(a)** 9-mm scan of the right eye of one participant (same subject as in Fig. 6) using the Cirrus 5000 HD-OCT. Only the nasal portion of the scan is shown here. **(b)** Digital magnification of the retinal region at the edge of the blind spot. Superimposed is the psychometric estimation of visibility obtained using our method. The red arrow indicates the position at which the photoreceptor layer breaks off.

transition zones, as they would only shifts psychometric functions. Thus, under the plausible assumption that subjects adopt similar response criteria at all tested eccentricities around the edge, the inter-subject variability that we report in the slope of the transition zone appears to be caused by differences in the underlying physiological substrate rather than in the categorization procedure.

Since our eye tracker only measured horizontal and vertical gaze displacements, the only movement that was not compensated in our experiments was the torsional rotation of the eye. This remaining oculomotor confound may have influenced our measurements, particularly given that torsional instability is considerable during sustained fixation, even in the absence of microsaccades (Ferman, Collewijn, Jansen, & Van den Berg, 1987; Van Rijn, Van Der Steen, & Collewijn, 1994). The measurements on the horizontal meridian reported in Fig. 3 were likely not affected by this residual smearing on the retina. But the typically reported torsional instability of a quarter of a degree would result in several arcminutes of uncertainty on the vertical meridian and may have influenced the measurements of Fig. 5. These residual errors are, however, too small to account for the estimated widths of the transition zones. Thus, the gradual visibility transitions we measured are unlikely to result from the residual smearing of sharp edges; they appear, instead, to reflect a genuine progressive decrement in visibility.

As expected from retinal anatomy, there is large variability in size and location of the blind spot across participants. However, while the precise anatomical characteristics of the blind spot differ, the relations among these properties tend to remain consistent. For example, the widths of the temporal and nasal borders both correlate with the eccentricity of the blind spot center. This correlation could be caused by the eccentricity-dependent changes in the tiling of photoreceptors and projections to retinal ganglion cells. Preliminary evidence from OCT imaging in one participant appears consistent with this interpretation. These images showed that the probe position corresponding to chance level detection roughly coincided with the retinal position at which the photoreceptor layer ended. However, detailed inspection indicates that detection goes below chance level shortly after the visible layer of photoreceptor is disrupted, pointing at the possible action of lateral connections in the retina or beyond. Related to this point, one might also expect the temporal border—in visual field coordinates—to be broader because of the decrease of resolution with eccentricity, since this border is located further peripherally than the nasal one. However, this was not the case in our data, suggesting that any potential difference between the two, if present, is small.

In two participants, we also determined the vertical borders of the blind spot, the axis of longest elongation (Safran et al., 1993). These data showed vast differences in the dimensions of the transition zones at the two edges. A detailed two-dimensional mapping of the blind spot in one participant confirmed that the width of the transition zone varies substantially around the blind spot. Fundus and OCT images showed that the reason for this variation is the presence of capillaries at these locations. This confirms the precision of our method, which is capable of mapping capillaries directly from psychophysical assessments.

Given the extent of the transition zones that we measured, the question emerges of whether the gradual decrease in visibility along the border is functionally relevant. The widths of these regions is much wider than the minimal stimulus frame needed to produce filling-in. Spillmann, Otte, Hamburger, and Magnussen (2006) showed that a rim of only 0.05° width placed around the blind spot suffices to produce at least partial filling-in of color. This previous study did not measure where exactly these very thin stimuli were placed, but the results suggest that partial activation of the border region might be sufficient. This process may be driven by the residual visibility in the transition region, particularly if eye movements take the stimulus inside and outside this zone. Fixational eye movements could also contribute by temporally modulating the responses of neurons within the transition zone. These modulations have been shown to strongly drive visual sensitivity outside the blind spot region (Rucci et al., 2007; Mostofi, Boi, & Rucci, 2016; Intoy & Rucci, 2020), discard redundant information in natural scenes (Kuang, Poletti, Victor, & Rucci, 2012; Mostofi et al., 2020) and enhance synchronous neural responses to non-redundant features in models (Rucci & Casile, 2004; Desbordes & Rucci, 2007; Casile, Victor, & Rucci, 2019). These previous findings raise the hypothesis that oculomotor-induced modulations within or around the transition zones could play a role in the process of filling-in, in much the same way that absence of luminance modulations leads to filling-in of large portions of the visual field when stationary stimuli are viewed under retinal stabilization (Ditchburn & Ginsborg, 1952; Riggs & Ratliff, 1952; Yarbus, 1967;

Poletti & Rucci, 2010).

In sum, we have presented in this study a new method for precise measurement of the border of visibility that surrounds the blind spot. This method relies on the presentation of probes at desired locations under stabilization, a technique that can be flexibly implemented by coupling gaze-contingent display control with precise eye-tracking. The approach allows definition of the blind spot's transition zone psychophysically within a few arcminutes, a level of resolution sufficient for quantitatively investigating visual functions and the mechanisms responsible for perceptual filling-in around the blind spot. The resolution of this method may also carry benefits in clinical settings. Changes in visibility around the blind spot have been reported in various conditions, including glaucoma (Coughlan & Friedmann, 1981; Haefliger & Flammer, 1989; Su, Park, Simonson, Liebmann, & Ritch, 2013). Our method enables detection of small functional changes around the optic nerve, which may go unnoticed in standard anatomical exams.

Declaration of Competing Interest

The authors declare that they have no known competing financial interests or personal relationships that could have appeared to influence the work reported in this paper.

Data availability

The data that support the findings of this study are available from the corresponding author upon reasonable request.

Acknowledgement

This work received funding from the European Union Horizon 2020 research and innovation program (Marie Skodowska-Curie grant agreement No 734227) and National Institute of Health grants EY018363 and P30 EY001319.

References

Armaly, M. F. (1969). The size and location of the normal blind spot. *Archives of Ophthamology, 81*(2), 192–201.
Awater, H., Kerlin, J. R., Evans, K. K., & Tong, F. (2005). Cortical representation of space around the blind spot. *Journal of Neurophysiology, 94*(5), 3314–3324.
Azzi, J., Gattass, R., Lima, B., Soares, J. G. M., & Fiorani, M. (2015). Precise visuotopic organization of the blind spot representation in primate V1. *Journal of Neurophysiology, 113*(10), 3588–3599.
Casile, A., Victor, J. D., & Rucci, M. (2019). Contrast sensitivity reveals an oculomotor strategy for temporally encoding space. *eLife*, 8:e40924.
Chamlin, M. (1960). Fluctuations in size of the normal blind spot. *Archives of Ophthalmology, 64*(4), 522–527.
Chen, N., Shin, K., Millin, R., Song, Y., Kwon, M., & Tjan, B. S. (2019). Cortical reorganization of peripheral vision induced by simulated central vision loss. *Journal of Neuroscience, 39*(18), 3529–3536.
Cherici, C., Kuang, X., Poletti, M., & Rucci, M. (2012). Precision of sustained fixation in trained and untrained observers. *Journal of Vision, 12*(6).
Coughlan, M. & Friedmann, A. I. (1981). The frequency distribution of early visual field defects in glaucoma. In E.L. Greve, G. Verriest (Eds.) Fourth international visual field symposium Bristol, April 13–16,1980. Documenta Ophthalmologica Proceedings Series, vol 26. Springer, Dordrecht.
Crane, H. D., & Steele, C. M. (1985). Generation-V dual-Purkinje-image eyetracker. *Applied Optics, 24*(4), 527–537.
Ditchburn, R. W., & Ginsborg, B. L. (1952). Vision with a stabilized retinal image. *Nature, 170*, 36–37.
Desbordes, G., & Rucci, M. (2007). A model of the dynamics of retinal activity during natural visual fixation. *Visual Neuroscience, 24*, 217–230.
Dolderer, J., Vontheim, R., Johnson, C. A., Schiefer, U., & Hart, W. (2006). Scotoma mapping by semi- automated kinetic perimetry: The effects of stimulus properties and the speed of subjects' responses. *Acta Ophthalmologica Scandinavica, 84*(3), 338–344.
Fang, Y., C., G., M., P., & Rucci, M. (2018). Monocular microsaccades: Do they really occur? *Journal of Vision*, 18(3): (pp. 18–18).
Ferman, L., Collewijn, H., Jansen, T. C., & Van den Berg, A. V. (1987). Human gaze stability in the horizontal, vertical and torsional direction during voluntary head movements, evaluated with a three-dimensional scleral induction coil technique. *Vision Research, 27*, 811–828.
Fiorani, M., Rosa, M. G. P., Gattass, R., & Rocha-Miranda, C. E. (1992). Dynamic surrounds of receptive fields in primate striate cortex: A physiological basis for perceptual completion? *Proceedings of the National Academy of Science, 89*(18), 8547–8551.
Haefliger, I. O., & Flammer, J. (1989). Fluctuation of the differential light threshold at the border of absolute scotomas. Comparison between glaucomatous visual field defects and blind spots. *Ophthalmology, 98*(10), 1529–1532.
Intoy, J., & Rucci, M. (2020). Finely tuned eye movements enhance visual acuity. *Nature Communications, 11*(795), 1–11.
Ko, H. K., Poletti, M., & Rucci, M. (2010). Microsaccades precisely relocate gaze in a high visual acuity task. *Nature Neuroscience, 13*(12), 1549–1553.
Ko, H. K., Snodderly, D. M., & Poletti, M. (2016). Eye movements between saccades: Measuring ocular drift and tremor. *Vision Research, 122*, 93–104.
Komatsu, H., Kinoshita, M., & Murakami, I. (2000). Neural responses in the retinotopic representation of the blind spot in the Macaque V1 to stimuli for perceptual filling-in. *Journal of Neuroscience, 20*(24), 9310–9319.
Komatsu, H. (2006). The neural mechanisms of perceptual filling-in. *Nature Reviews Neuroscience, 7*, 220–231.
Kowler, E. (2011). Eye movements: The past 25 years. *Vision Research, 51*, 1457–1483.
Krauskopf, J., Cornsweet, T. N., & Riggs, L. A. (1960). Analysis of eye movements during monocular and binocular fixation. *Journal of the Optical Society of America, 50*(6), 572–578.
Kuang, X., Poletti, M., Victor, J. D., & Rucci, M. (2012). Temporal encoding of spatial information during active visual fixation. *Current Biology, 22*(6), 510–514.
Meyer, J. H., Guhlmann, M., & Funk, J. (1997). Blind spot size depends on the optic disc topography: A study using SLO controlled scotometry and the Heidelberg retina tomograph. *British Journal of Ophthalmology, 81*, 355–359.
Maus, G. W., & Nijhawan, R. (2008). Motion extrapolation into the blind spot. *Psychological Science, 19*(11), 1087–1091.
Maus, G. W., & Whitney, D. (2016). Motion-dependent filling-in of spatiotemporal information at the blind spot. *PLoS One, 11*(4), e0153896.
Mostofi, N., Boi, M., & Rucci, M. (2016). Are the visual transients from microsaccades helpful? Measuring the influences of small saccades on contrast sensitivity. *Vision Research, 118*, 60–69.
Mostofi, N., Zhao, Z., Intoy, J., Boi, M., Victor, J. D., & Rucci, M. (2020). Spatiotemporal content of saccade transients. *Current Biology, 30*(20), 3999–4008.
Murakami, I., Komatsu, H., & Kinoshita, M. (1997). Perceptual filling-in at the scotoma following a monocular retinal lesion in the monkey. *Visual Neuroscience, 14*(1), 89–101.
Poletti, M., & Rucci, M. (2010). Eye movements under various conditions of image fading. *Journal of Vision, 10*(3), 1–18.
Poletti, M., Aytekin, M., & Rucci, M. (2015). Head-eye coordination at a microscopic scale. *Current Biology, 25*(24), 3253–3259.
Poletti, M., & Rucci, M. (2016). A compact field guide to the study of microsaccades: Challenges and functions. *Vision Research, 118*, 83–97.
Poletti, M., Intoy, J., & Rucci, M. (2020). Accuracy and precision of small saccades. *Scientific Reports, 10*, 16097.
Ramachandran, V. S., & Gregory, R. L. (1991). Perceptual filling in of artificially induced scotomas in human vision. *Nature, 350*, 699–702.
Ramachandran, V. S. (1992). Filling in the blind spot. *Nature, 356*(6365), 115.
Raman, R., & Sarkar, S. (2016). Predictive coding: a possible explanation of filling-in at the blind spot. *PLoS ONE, 11*(3), e0151194.
Rhodes, M. (2013). A systematic review: What is the normative size of the blind spot scotoma in human adults? *Ophthalmology Research: An International Journal, 1*(1), 51–66.
Riggs, L. A., & Ratliff, F. (1952). The effects of counteracting the normal movements of the eye. *Journal of the Optical Society of America, 42*, 872–873.
Rolfs, M. (2009). Microsaccades: small steps on a long way. *Vision Research, 49*, 2415–2441.
Rucci, M., & Casile, A. (2004). Decorrelation of neural activity during fixational instability: Possible implications for the refinement of V1 receptive fields. *Visual Neuroscience, 21*, 725–738.
Rucci, M., Iovin, R., Poletti, M., & Santini, F. (2007). Miniature eye movements enhance fine spatial detail. *Nature, 447*(7146), 852–855.
Rucci, M., & Poletti, M. (2015). Control and functions of fixational eye movements. *Annual Review of Vision Science, 1*, 499–518.
Safran, A.B., B., M., Mermoud, C., Weisse, C.D., & Desangles, D. (1993). Characteristic features of blind spot size and location, when evaluated with automated perimetry: Values obtained in normal subjects. *Neuro-ophthamology* 13(6): (pp. 309–315).
Santini, F., Redner, G., Iovin, R., & Rucci, M. (2007). EyeRIS: a general-purpose system for eye-movement-contingent display control. *Behavioural Research Methods, 39*(3), 350–364.
Spillmann, L. (2006). From perceptive fields to Gestalt. *Progress in Brain Research, 155*, 67–92.
Spillmann, L., Otte, T., Hamburger, K., & Magnussen, S. (2006). Perceptual filling-in from the edge of the blind spot. *Vision Research, 46*(25), 4252–4257.
Stefani, E. D., Pinello, L., Campana, G., Mazzarolo, M., Giudice, G. L., & Casco, C. (2011). Illusory contours over pathological retinal scotomas. *PLoS ONE, 6*(10), e26154.
Su, D., Park, S. C., Simonson, J. L., Liebmann, J. M., & Ritch, R. (2013). Progression pattern of initial parafoveal scotomas in glaucoma. *Ophthalmology, 120*(3), 520–527.
Van Rijn, L. J., Van Der Steen, J., & Collewijn, H. (1994). Instability of ocular torsion during fixation: Cyclovergence is more stable than cycloversion. *Vision Research, 34*(8), 1077–1087.
Weil, R. S., Kilner, J. M., Haynes, J. D., & Rees, G. (2007). Neural correlates of perceptual filling-in of an artificial scotoma in humans. *Proceedings of the National Academy of Sciences, 104*(12), 5211–5216.

Wittich, W., Overbury, O., Kapusta, M. A., Watanabe, D. H., & Faubert, J. (2006). Macular hole: perceptual filling-in across central scotomas. *Vision Research, 46*, 4064–4070.
Wichmann, F. A., & Hill, N. J. (2001a). The psychometric functions: I. Fitting, sampling and goodness of fit. *Perception and Psychophysics, 63*, 1293–1313.
Wichmann, F. A., & Hill, N. J. (2001b). The psychometric functions: II. Bootstrap-based confidence intervals and sampling. *Perception and Psychophysics, 63*, 1214–1329.
Wu, R.-J., Clark, A. M., Cox, M. A., Intoy, J., Jolly, P. C., Zhao, Z., & Rucci, M. (2023). High-resolution eye-tracking via digital imaging of Purkinje reflections. *J. Vis., 23* (5), 4. https://doi.org/10.1167/jov.23.5.4
Wyatt, H. J., Dul, M. W., & Swanson, W. H. (2007). Variability of visual field measurements is correlated with the gradient of visual sensitivity. *Vision Research, 47*, 925–936.
Yarbus, A. L. (1967). *Eye movements and vision*. New York: Plenum Press.
Zur, D., & Ullman, S. (2003). Filling-in of retinal scotomas. *Vision Research, 43*, 971–982.